

**SYNTHESIS, CHARACTERIZATION AND DNA  
CLEAVAGE ABILITY OF COBALT(II) AND ZINC(II)  
COMPLEXES**

**by**

**GOH SIU MUN**

**Thesis submitted in fulfillment of the requirement**

**for the degree of**

**Master of Science**

## ACKNOWLEDGEMENT

First and the most, I would like to take this opportunity to thank and acknowledge my supervisor, Prof. Dr. Teoh Siang Guan, for his support, guidance, inspiration, enthusiasm and help. I would also like to acknowledge the Dean of Institute of Graduate Studies(IPS) for giving me a chance to further my postgraduate studies in USM. Not forgetting, special thanks to the Dean of School of Chemical Sciences, Prof. Dr. Wan Ahmad Kamil Che Mahmood for providing me all the assistance and facilities which ensured the success of my research.

I would like to acknowledge Dr. Tang Thean Hock of Advanced Medical and Dental Institute and Dr. Alexander Chong Shu Chien of School of Biological Sciences, USM for their advice and help in the biological activities study. I am also grateful to Prof. Dr. Fun Hoong Kun of School of Physics, USM for his help and advice in single crystal X-ray structural determination.

Next, I would like to thank to all the laboratory assistants, Mr. Aw Yeong Cheok Hoe (FTIR Analysis), Mr. Ong Chin Hin, Mr. Razly Effendy (CHN Analysis), Mr. Marimuthu (AAS Analysis) and Mr. Burhanuddin Saad (TGA) for being so patient and lead me a helping hand each time experiments are conducted.

Here, I would like to thank IPS again for awarding me the Graduate Assitanship (Teaching) (GA) followed by USM Fellowship which covered my tuition fees and my allowances. Next, I would like to thank the technical staffs of the School of Chemical Sciences, School of Physics and School of Biological Sciences for their help in my study.

I would like to forward my appreciation to all my friends in USM in particular Cynn Dee, Eng Khoon, William, Naser, Sharon, Chin Hin, Guat Siew and

for their guidance, moral support and encouragement. I also would like to convey my love and deepest gratitude to my family members for their care, love, encouragement and understanding throughout my candidature.

Finally, my sincere appreciation for those who have given me help, advice and guidance directly or indirectly during my study and candidature.

## TABLE OF CONTENTS

	<i>Page</i>
Acknowledgement	ii
Table of contents	iv
List of abbreviations	x
List of tables	xii
List of figures	xv
Abstrak	xxxviii
Abstract	xl
 <b>CHAPTER ONE: INTRODUCTION</b>	
1.1 DNA	1
1.2 Metals used as DNA cleaving agents	3
1.3 Usage and application of cobalt complexes	5
1.4 Cobalt in antitumor complexes	6
1.5 Usage and application of zinc complexes	8
1.6 Zinc in antitumor complexes	9
1.7 Mechanism of DNA cleavage	
1.7.1 Reactive oxygen species (ROS)	10
1.7.2 Carbon centered radicals	12
1.8 Fenton-Menton reaction	13
1.9 MTT assay	14
1.10 IC <sub>50</sub>	15
1.11 Objectives and scope of study	16

## CHAPTER 2 : MATERIALS AND METHODS

2.1	Reagents	17
2.2	Experimental	
2.3	Methods of characterization	
2.3.1	Melting points	18
2.3.2	Conductivity measurement	19
2.3.3	Fourier transform infrared spectroscopy (FT-IR) analysis	19
2.3.4	Microanalysis CHN	19
2.3.5	Atomic absorption spectrometry (AAS) analysis	19
2.3.6	Ultraviolet-visible spectrometry (UV-Vis) analysis	19
2.3.7	Cyclic voltammetry (CV) analysis	19
2.3.8	Thermogravimetric (TGA) analysis	20
2.3.9	X-ray crystallography	21
2.3.10	DNA cleavage experiments	22
2.3.11	MTT assay	22

## CHAPTER 3 : RESULTS AND DISCUSSION

3.1	Characterization of diaquabis(2-pyrazinecarboxylato)cobalt(II) and diaquabis(2-pyrazinecarboxylato)zinc(II)	
3.1.1	Determination of physical properties	24
3.1.2	Fourier transform infrared spectroscopy (FT-IR) analysis	25

3.1.3	Microanalysis using CHN and AAS	30
3.1.4	Ultraviolet-visible spectroscopy (UV-Vis) analysis	31
3.1.5	Cyclic voltammetry (CV) analysis	33
3.1.6	Thermogravimetry (TGA) analysis	35
3.1.7	Structure postulation and X-ray crystallography	40
3.2	Biological Properties	
3.2.1.	Cleavage of DNA in tris-HCl buffer pH 4.5	43
3.2.2	Possible mechanism	45
3.2.3	MTT assay	48
3.3	Characterization of tetraaquabis(maleato)cobalt(II) and tetraaquabis(maleato)zinc(II)	
3.3.1	Determination of physical properties	50
3.3.2	Fourier transform infrared spectroscopy (FT-IR) analysis	51
3.3.3	Microanalysis using CHN and AAS	54
3.3.4	Ultraviolet-visible spectroscopy (UV-Vis) analysis	55
3.3.5	Cyclic voltammetry (CV) analysis	57
3.3.6	Thermogravimetry (TGA) analysis	58
3.3.7	Structure postulation and X-ray crystallography	65
3.4	Biological Properties	
3.4.1	Cleavage of DNA in tris-HCl buffer pH 4.5	67
3.4.2	Possible mechanism	69
3.4.3	MTT assay	71

3.5	Characterization of diaquabis(picolinato)cobalt(II)dihydrate and diaquabis(picolinato)zinc(II)dihydrate	
3.5.1	Determination of physical properties	73
3.5.2	Fourier transform infrared spectroscopy (FT-IR) analysis	
3.5.3	Microanalysis using CHN and AAS	77
3.5.4	Ultraviolet-visible spectroscopy (UV-Vis) analysis	78
3.5.5	Cyclic voltammetry (CV) analysis	80
3.5.6	Thermogravimetry (TGA) analysis	81
3.5.7	Structure postulation and X-ray crystallography	90
3.6	Biological Properties	
3.6.1	Cleavage of DNA in tris-HCl buffer pH 4.5	92
3.6.2	Possible mechanism	94
3.6.3	MTT assay	96
3.7	Characterization of diaquabis(malonato)cobalt(II) and diaquabis (malonato)zinc(II)	
3.7.1	Determination of physical properties	98
3.7.2	Fourier transform infrared spectroscopy (FT-IR) analysis	99
3.7.3	Microanalysis using CHN and AAS	102
3.7.4	Ultraviolet-visible spectroscopy (UV-Vis) analysis	103
3.7.5	Cyclic voltammetry (CV) analysis	105

3.7.6	Thermogravimetry (TGA) analysis	106
3.7.7	Structure postulation and X-ray crystallography	111
3.8	Biological properties	
3.8.1	Cleavage of DNA in tris-HCl buffer pH 4.5	113
3.8.2	Possible mechanism	115
3.8.3	MTT assay	117
3.9	Characterization of diaquadichloro(glycine)cobalt(II), bis(glycolato)cobalt(II), tetraaquabis(3,5- dinitrobenzoato)cobalt(II)tetrahydrate, diaquabis(pyridine- 2,3-dicarboxylato)cobalt(II), diaquabis(pyridine-2,5- dicarboxylato)cobalt(II) and diaquabis(4- aminobenzoato)cobalt(II)	
3.9.1	Determination of physical properties	119
3.9.2	Fourier transform infrared spectroscopy (FT-IR) analysis	121
3.9.3	Microanalysis using CHN and AAS	134
3.9.4	Ultraviolet-visible spectroscopy (UV-Vis) analysis	136
3.9.5	Cyclic voltammetry (CV) analysis	139
3.9.6	Thermogravimetry (TGA) analysis	143
3.9.7	Structure postulation and X-ray crystallography	161
3.10	Biological Properties	
3.10.1	Cleavage of DNA in tris-HCl buffer pH 4.5	167
3.10.2	Possible Mechanism	173
3.10.3	MTT assay	179



<b>CHAPTER 4 : CONCLUSION</b>	181
<b>FUTURE RESEARCH WORK</b>	183
<b>REFENCES</b>	184

## LIST OF ABBREVIATIONS

AAS = Atomic absorption spectroscopy

CHN = Carbon, hydrogen, nitrogen

Co(2-pc) = diaquabis(picolinato)cobalt(II)dihydrate

Co(3,5-dn) = tetraaquabis(3,5-dinitrobenzoato)cobalt(II)tetrahydrate

Co(4-amino) = diaquabis(4-aminobenzoato)cobalt(II)

Co(gly) = diaquadichloro(glycine)cobalt(II)

Co(glycol) = bis(glycolato)cobalt(II)

Co(mal) = diaquabis(malonato)cobalt(II)

Co(maleic) = tetraaquabis(maleato)cobalt(II)

Co(p-2c) = diaquabis(pyrazine-2-carboxylato)cobalt(II)

Co(pyd-2,5-dc) = diaquabis(pyridine-2,5-dicarboxylato)cobalt(II)

Co(quino) = diaquabis(pyridine-2,3-dicarboxylato)cobalt(II)

CoCl<sub>2</sub>·6H<sub>2</sub>O = cobalt(II)chloride hexahydrate

CV = Cyclic voltammetry

DMSO = dimethyl sulfoxide

DNA = Deoxyribonucleic acid

FT-IR = Fourier transform infrared spectroscopy

H<sub>2</sub>O<sub>2</sub> = hydrogen peroxide

KI = potassium iodide

MTT = 3-(4,5-dimethylthiazol-2-yl)-2,5-diphenyltetrazolium bromide

NaN<sub>3</sub> = sodium azide

ROS = Reactive oxygen species

TGA = Thermogravimetric analysis

UV-Vis = Ultraviolet-visible spectrometry

Zn(2-pc) = diaquabis(picolinato)zinc(II)dihydrate

Zn(CH<sub>3</sub>COO)<sub>2</sub>·2H<sub>2</sub>O = zinc(II)acetate dihydrate

Zn(mal) = diaquabis(malonato)zinc(II)

Zn(maleic) = tetraaquabis(maleato)zinc(II)

Zn(p-2c) = diaquabis(pyrazine-2-carboxylato)zinc(II)

## LIST OF TABLES

	<i>Page</i>	
Table 2.1	Chemicals used in the research	17
Table 3.1. 1	The physical properties of Co(p-2c) and Zn(p-2c)	25
Table 3.1.2	Molar conductance, $\Lambda$ of electrolyte solution at 25°C	25
Table 3.1.3	Comparison of IR absorption bands of asymmetric and symmetric COO <sup>-</sup> stretchings	26
Table 3.1.4	Results of CHN and AAS of Co(p-2c) and Zn(p-2c) analyses	31
Table 3.1.5	Thermogravimetric results of Co(p-2c)	37
Table 3.1.6	Thermogravimetric results of Zn(p-2c)	39
Table 3.2.1	The IC <sub>50</sub> values of CoCl <sub>2</sub> ·6H <sub>2</sub> O, Zn(CH <sub>3</sub> COO) <sub>2</sub> ·2H <sub>2</sub> O, Co(p-2c) and Zn(p-2c) on HepG2	49
Table 3.3.1	The physical properties of Co(maleic) and Zn(maleic)	51
Table 3.3.2	Comparison of IR absorption bands of asymmetric and symmetric stretching COO <sup>-</sup>	54
Table 3.3.3	Results of CHN and AAS of Co(maleic) and Zn(maleic) analyses	55
Table 3.3.4	Thermogravimetric results of Co(maleic)	60
Table 3.3.5	Thermogravimetric results of Zn(maleic)	63
Table 3.4.1	The IC <sub>50</sub> values of Co(maleic) and Zn(maleic) on HepG2	72

Table 3.5.1	The physical properties of Co(p-2c) and Zn(p-2c)	73
Table 3.5.2	Comparison of IR absorption bands of asymmetric and symmetric stretching COO <sup>-</sup>	77
Table 3.5.3	The combination results of CHN and AAS of Co(2-pc) and Zn(2-pc)	78
Table 3.5.4	Thermogravimetric results of Co(2-pc)	84
Table 3.5.5	Thermogravimetric results of Zn(2-pc)	88
Table 3.6.1	The IC <sub>50</sub> values of Co(2-pc) and Zn(2-pc) on HepG2	97
Table 3.7.1	The physical properties of Co(mal) and Zn(mal)	98
Table 3.7.2	Comparison of IR absorption bands of asymmetric and symmetric stretching COO <sup>-</sup>	102
Table 3.7.3	Results of CHN and AAS of Co(mal) and Zn(mal) analyses	102
Table 3.7.4	Thermogravimetric results of Co(mal)	108
Table 3.7.5	Thermogravimetric results of Zn(mal)	110
Table 3.8.1	The IC <sub>50</sub> values of Co(mal) and Zn(mal) on HepG2	118
Table 3.9.1	Complexes that formed by the reaction of CoCl <sub>2</sub> ·6H <sub>2</sub> O with the following ligands are presented as below	119
Table 3.9.2	The physical properties of Co(gly), Co(glycol), Co(3,5-dn), Co(quino), Co(pyd-2,5-dc) and Co(4-amino)	120
Table 3.9.3	Comparison of IR absorption bands of asymmetric and symmetric stretching COO <sup>-</sup>	134

Table 3.9.4	Results of CHN and AAS of Co(gly), Co(glycol), Co(3,5-dn), Co(quino), Co(pyd-2,5-dc) and Co(4- amino) analyses	135
Table 3.9.5	Thermogravimetric results of Co(gly)	144
Table 3.9.6	Thermogravimetric results of Co(glycol)	147
Table 3.9.7	Thermogravimetric results of Co(3,5-dn)	150
Table 3.9.8	Thermogravimetric results of Co(quino)	153
Table 3.9.9	Thermogravimetric results of Co(pyd-2,5-dc)	156
Table 3.9.10	Thermogravimetric results of Co(4-amino)	159
Table 3.10.1	The IC <sub>50</sub> values of CoCl <sub>2</sub> ·6H <sub>2</sub> O, Co(gly), Co(glycol), Co(3,5-dn), Co(quino), Co(pyd-2,5-dc) and Co(4- amino) on HepG2	180

## LIST OF FIGURES

		<i>Page</i>
Figure 1.1	Double helix DNA	1
Figure 1.2	The chemical structure of DNA	2
Figure 1.3	Cisplatin	5
Figure 1.4	Schematic diagram showing metal ion conversion to hydroxyl radicals	11
Figure 1.5	Schematic representation for the reaction of guanine with hydroxyl radicals	12
Figure 1.6	Schematic representation of carbon centered metabolites where R represents a carbon radical	13
Figure 1.7	Mechanism of Fenton-Menton reaction (M represents metal)	14
Figure 1.8	The graph of $IC_{50}$	16
Figure 3.1.1	The monodentate coordination	26
Figure 3.1.2	IR spectrum of $Co(p-2c)$	28
Figure 3.1.3	IR spectrum of $Zn(p-2c)$	29
Figure 3.1.4	IR spectrum of pyrazine-2-carboxylic acid	29
Figure 3.1.5	IR spectrum of sodium pyrazine-2-carboxylate	30
Figure 3.1.6	UV-Vis spectra of $Co(p-2c)$	32
Figure 3.1.7	UV-Vis spectra of $Zn(p-2c)$	32
Figure 3.1.8	Voltammogram of $CoCl_2 \cdot 6H_2O$	33
Figure 3.1.9	Voltammogram of $Zn(CH_3COO)_2 \cdot 2H_2O$	34
Figure 3.1.10	Voltammogram of $Co(p-2c)$	34

Figure 3.1.11	Voltammogram of Zn(p-2c)	35
Figure 3.1.12	TGA curves of Co(p-2c)	36
Figure 3.1.13	The postulated decomposition pathway of Co(p-2c)	38
Figure 3.1.14	TGA curves of Zn(p-2c)	38
Figure 3.1.15	The postulated decomposition pathway of Zn(p-2c)	40
Figure 3.1.16	Postulated structure of diaquabis(2-pyrazinecarboxylato)cobalt(II), [Co(p2c)] (Ptasiewicz-Bak <i>et al.</i> , 1995)	41
Figure 3.1.17	Postulated structure of diaquabis(2-pyrazinecarboxylato)zinc(II), [Zn(p-2c)] (Ptasiewicz-Bak <i>et al.</i> , 1995)	41
Figure 3.1.18	Molecular structure of diaquabis(2-pyrazinecarboxylato)zinc(II), [Zn(p-2c)] (Ptasiewicz-Bak <i>et al.</i> , 1995)	42



Figure 3.2.1 Agarose (1%) gel electrophoresis banding patterns 44  
of plasmid pBR322 ( $0.025\mu\text{g } \mu\text{L}^{-1}$ ) treated with  
various concentration of Co(p-2c) in the presence  
of 2mM  $\text{H}_2\text{O}_2$  and Tris-HCl buffer pH 4.5. Lane  
1, Gene ruler 1kb DNA ladder; Lane 2, DNA  
alone; Lane 3,  $\text{H}_2\text{O}_2$  alone; Lane 4, DNA+1.0mM  
Co(p-2c); Lane 5–12 involve DNA+2mM  
 $\text{H}_2\text{O}_2$ +different concentration of Co(p-2c): Lane  
5, 0.3mM; Lane 6, 0.4mM; Lane 7, 0.5mM; Lane  
8, 0.6mM; Lane 9, 0.7mM; Lane 10, 0.8mM; Lane  
11, 0.9mM; Lane 12, 1.0mM.

Figure 3.2.2 Agarose (1%) gel electrophoresis banding patterns 45  
of plasmid pBR322 ( $0.025\mu\text{g } \mu\text{L}^{-1}$ ) treated with  
various concentration of Zn(p-2c) in the presence  
of 2mM  $\text{H}_2\text{O}_2$  and Tris-HCl buffer pH 4.5. Lane  
1, Gene ruler 1kb DNA ladder; Lane 2, DNA  
alone; Lane 3,  $\text{H}_2\text{O}_2$  alone; Lane 4, DNA+7.5mM  
Zn(p-2c); Lane 5–12 involve DNA+2mM  
 $\text{H}_2\text{O}_2$ +different concentration of Zn(p-2c): Lane  
5, 6.8mM; Lane 6, 6.9mM; Lane 7, 7.0mM; Lane  
8, 7.1mM; Lane 9, 7.2mM; Lane 10, 7.3mM; Lane  
11, 7.4mM; Lane 12, 7.5mM.

- Figure 3.2.3      Effect of hydroxyl radicals scavengers and singlet oxygen scavengers on the DNA cleavage of pBR322 ( $0.025\mu\text{g } \mu\text{L}^{-1}$ ) by 0.8mM of Co(p-2c) in the presence of 2mM  $\text{H}_2\text{O}_2$ . Lane 1, Gene ruler 1 kb DNA ladder; Lane 2, DNA alone; Lane 3,  $\text{H}_2\text{O}_2$  alone; Lane 4, DNA+0.8mM Co(p-2c)+2mM  $\text{H}_2\text{O}_2$ ; Lane 5–10, involve DNA+2mM  $\text{H}_2\text{O}_2$ +0.8mM Co(p-2c) in the presence of various scavengers: Lane 5, 2mM DMSO; Lane 6, 2mM D-Mannitol; Lane 7, 2mM t-butanol; Lane 8, 2mM KI; Lane 9, 1mM  $\text{NaN}_3$ ; Lane 10, 1.5mM  $\text{NaN}_3$ .      46
- Figure 3.2.4      Effect of hydroxyl radicals scavengers and singlet oxygen scavengers on the DNA cleavage of pBR322 ( $0.025\mu\text{g } \mu\text{L}^{-1}$ ) by 7.3mM of Zn(p-2c) in the presence of 2mM  $\text{H}_2\text{O}_2$ . Lane 1, Gene ruler 1 kb DNA ladder; Lane 2, DNA alone; Lane 3,  $\text{H}_2\text{O}_2$  alone; Lane 4, DNA+7.3mM Zn(p-2c)+2mM  $\text{H}_2\text{O}_2$ ; Lane 5–10, involve DNA+2mM  $\text{H}_2\text{O}_2$ +7.3mM Zn(p-2c) in the presence of various scavengers: Lane 5, 2mM DMSO; Lane 6, 2mM D-Mannitol; Lane 7, 2mM t-butanol; Lane 8, 2mM KI; Lane 9, 1mM  $\text{NaN}_3$ ; Lane 10, 1.5mM  $\text{NaN}_3$ .      48
- Figure 3.3.1      IR spectrum of Co(maleic)      52

Figure 3.3.2	IR spectrum of Zn(maleic)	53
Figure 3.3.3	IR spectrum of maleic acid	53
Figure 3.3.4	IR spectrum of sodium maleate	54
Figure 3.3.5	UV-Vis spectrum of Co(maleic)	56
Figure 3.3.6	UV-Vis spectrum of Zn(maleic)	56
Figure 3.3.7	Voltammogram of Co(maleic)	57
Figure 3.3.8	Voltammogram of Zn(maleic)	58
Figure 3.3.9	TGA curves of Co(maleic)	59
Figure 3.3.10	The postulated decomposition diagram of Co(maleic)	61
Figure 3.3.11	TGA of Zn(maleic)	62
Figure 3.3.12	The postulated decomposition diagram of Zn(maleic)	64
Figure 3.3.13	Postulated structure of tetraaquabis(maleato)cobalt(II), [Co(maleic)] (Sawhney <i>et al.</i> , 1985)	65
Figure 3.3.14	Molecular structure of tetraaquabis(maleato)cobalt(II), [Co(maleic)] (Sawhney <i>et al.</i> , 1985)	65
Figure 3.3.15	Postulated structure of tetraaquabis(maleato)zinc(II), [Zn(maleic)] (Sequeira <i>et al.</i> , 1992)	66
Figure 3.3.16	Molecular structure of tetraaquabis(maleato)zinc(II), [Zn(maleic)] (Sequeira <i>et al.</i> , 1992)	66

Figure 3.4.1 Agarose (1%) gel electrophoresis banding patterns of plasmid pBR322 ( $0.025 \mu\text{g}\mu\text{L}^{-1}$ ) treated with various concentration of Co(maleic) in the presence of  $2 \text{ mM H}_2\text{O}_2$  and Tris-HCl buffer pH 4.5. Lane 1, Gene ruler 1 kb DNA ladder; Lane 2, DNA alone; Lane 3,  $\text{H}_2\text{O}_2$  alone; Lane 4, DNA+ $6.5 \text{ mM Co(maleic)}$ ; Lane 5–12 involve DNA+ $2 \text{ mM H}_2\text{O}_2$ +different concentration of Co(maleic): Lane 5,  $2.5 \text{ mM}$ ; Lane 6,  $3.0 \text{ mM}$ ; Lane 7,  $3.5 \text{ mM}$ ; Lane 8,  $4.0 \text{ mM}$ ; Lane 9,  $4.5 \text{ mM}$ ; Lane 10,  $5.5 \text{ mM}$ ; Lane 11,  $6.0 \text{ mM}$ ; Lane 12,  $6.5 \text{ mM}$ . 68

Figure 3.4.2 Agarose (1%) gel electrophoresis banding patterns of plasmid pBR322 ( $0.025 \mu\text{g}\mu\text{L}^{-1}$ ) treated with various concentration of Zn(maleic) in the presence of  $2 \text{ mM H}_2\text{O}_2$  and Tris-HCl buffer pH 4.5. Lane 1, Gene ruler 1kb DNA ladder; Lane 2, DNA alone; Lane 3,  $\text{H}_2\text{O}_2$  alone; Lane 4, DNA+ $9.0 \text{ mM Zn(maleic)}$ ; Lane 5–12 involve DNA+ $2 \text{ mM H}_2\text{O}_2$ +different concentration of Zn(maleic): Lane 5,  $8.3 \text{ mM}$ ; Lane 6,  $8.4 \text{ mM}$ ; Lane 7,  $8.5 \text{ mM}$ ; Lane 8,  $8.6 \text{ mM}$ ; Lane 9,  $8.7 \text{ mM}$ ; Lane 10,  $8.8 \text{ mM}$ ; Lane 11,  $8.9 \text{ mM}$ ; Lane 12,  $9.0 \text{ mM}$ . 69

- Figure 3.4.3      Effect of hydroxyl radicals scavengers and singlet oxygen scavengers on the DNA cleavage of pBR322 ( $0.025 \mu\text{g}\mu\text{L}^{-1}$ ) by 4.0 mM of Co(maleic) in the presence of 2 mM  $\text{H}_2\text{O}_2$ . Lane 1, Gene ruler 1 kb DNA ladder; Lane 2, DNA alone; Lane 3,  $\text{H}_2\text{O}_2$  alone; Lane 4, DNA+4.0 mM Co(maleic)+2 mM  $\text{H}_2\text{O}_2$ ; Lane 5–10, involve DNA+2 mM  $\text{H}_2\text{O}_2$ +4.0 mM Co(maleic) in the presence of various scavengers: Lane 5, 2 mM DMSO; Lane 6, 2 mM D-Mannitol; Lane 7, 2 mM t-butanol; Lane 8, 2 mM KI; Lane 9, 1 mM  $\text{NaN}_3$ ; Lane 10, 1.5 mM  $\text{NaN}_3$ .      70
- Figure 3.4.4      Effect of hydroxyl radicals scavengers and singlet oxygen scavengers on the DNA cleavage of pBR322 ( $0.025\mu\text{g} \mu\text{L}^{-1}$ ) by 8.9mM of Zn(maleic) in the presence of 2mM  $\text{H}_2\text{O}_2$ . Lane 1, Gene ruler 1 kb DNA ladder; Lane 2, DNA alone; Lane 3,  $\text{H}_2\text{O}_2$  alone; Lane 4, DNA+8.9mM Zn(maleic)+2mM  $\text{H}_2\text{O}_2$ ; Lane 5–10, involve DNA+2mM  $\text{H}_2\text{O}_2$ +8.9mM Zn(maleic) in the presence of various scavengers: Lane 5, 2mM DMSO; Lane 6, 2mM D-Mannitol; Lane 7, 2mM t-butanol; Lane 8, 2mM KI; Lane 9, 1mM  $\text{NaN}_3$ ; Lane 10, 1.5mM  $\text{NaN}_3$ .      71
- Figure 3.5.1      IR spectrum of Co(2-pc)      75

Figure 3.5.2	IR spectrum of Zn(2-pc)	76
Figure 3.5.3	IR spectrum of 2-picolinic acid	76
Figure 3.5.4	IR spectrum of sodium 2-piconate	77
Figure 3.5.5	UV-Vis spectrum of Co(2-pc)	79
Figure 3.5.6	UV-Vis spectrum of Zn(2-pc)	79
Figure 3.5.7	Voltammogram of Co(2-pc)	80
Figure 3.5.8	Voltammogram of Zn(2-pc)	81
Figure 3.5.9	TGA curves of Co(2-pc)	82
Figure 3.5.10	Enlarge TGA curves of Co(2-pc)	83
Figure 3.5.11	The postulated decomposition diagram of Co(2-pc)	85
Figure 3.5.12	TGA curves of Zn(2-pc)	86
Figure 3.5.13	Enlarge TGA curves of Zn(2-pc)	87
Figure 3.5.14	The postulated decomposition diagram of Zn(2-pc)	89
Figure 3.5.15	Postulated structure of diaquabis(picolinato)cobalt(II)dihydrate, [Co(2-pc)] (Heren <i>et al.</i> , 2006)	90
Figure 3.5.16	Postulated structure of diaquabis(picolinato)zinc(II)dihydrate, [Zn(2-pc)], (Li <i>et al.</i> , 2008)	91

Figure 3.6.1 Agarose (1%) gel electrophoresis banding patterns of plasmid pBR322 ( $0.025 \mu\text{g}\mu\text{L}^{-1}$ ) treated with various concentration of Co(2-pc) in the presence of 2 mM  $\text{H}_2\text{O}_2$  and Tris-HCl buffer pH 4.5. Lane 1, Gene ruler 1 kb DNA ladder; Lane 2, DNA alone; Lane 3,  $\text{H}_2\text{O}_2$  alone; Lane 4, DNA+1.6 mM Co(2-pc); Lane 5–12 involve DNA+2 mM  $\text{H}_2\text{O}_2$ +different concentration of Co(2-pc): Lane 5, 0.9 mM; Lane 6, 1.0 mM; Lane 7, 1.1 mM; Lane 8, 1.2 mM; Lane 9, 1.3 mM; Lane 10, 1.4 mM; Lane 11, 1.5 mM; Lane 12, 1.6 mM. 93

Figure 3.6.2 Agarose (1%) gel electrophoresis banding patterns of plasmid pBR322 ( $0.025 \mu\text{g}\mu\text{L}^{-1}$ ) treated with various concentration of Zn(2-pc) in the presence of 2 mM  $\text{H}_2\text{O}_2$  and Tris-HCl buffer pH 4.5. Lane 1, Gene ruler 1 kb DNA ladder; Lane 2, DNA alone; Lane 3,  $\text{H}_2\text{O}_2$  alone; Lane 4, DNA+7.0 mM Zn(2-pc); Lane 5–12 involve DNA+2 mM  $\text{H}_2\text{O}_2$ +different concentration of Zn(2-pc): Lane 5, 6.3 mM; Lane 6, 6.4 mM; Lane 7, 6.5 mM; Lane 8, 6.6 mM; Lane 9, 6.7 mM; Lane 10, 6.8 mM; Lane 11, 6.9mM; Lane 12, 7.0mM. 94

- Figure 3.6.3      Effect of hydroxyl radicals scavengers and singlet oxygen scavengers on the DNA cleavage of pBR322 ( $0.025 \mu\text{g}\mu\text{L}^{-1}$ ) by 1.1 mM of Co(2-pc) in the presence of 2 mM  $\text{H}_2\text{O}_2$ . Lane 1, Gene ruler 1 kb DNA ladder; Lane 2, DNA alone; Lane 3,  $\text{H}_2\text{O}_2$  alone; Lane 4, DNA+1.1 mM Co(2-pc)+2 mM  $\text{H}_2\text{O}_2$ ; Lane 5–10, involve DNA+2 mM  $\text{H}_2\text{O}_2$ +1.1 mM Co(2-pc) in the presence of various scavengers: Lane 5, 2 mM DMSO; Lane 6, 2 mM D-Mannitol; Lane 7, 2 mM t-butanol; Lane 8, 2 mM KI; Lane 9, 1 mM  $\text{NaN}_3$ ; Lane 10, 1.5 mM  $\text{NaN}_3$ .      95
- Figure 3.6.4      Effect of hydroxyl radicals scavengers and singlet oxygen scavengers on the DNA cleavage of pBR322 ( $0.025 \mu\text{g}\mu\text{L}^{-1}$ ) by 6.5 mM of Zn(2-pc) in the presence of 2 mM  $\text{H}_2\text{O}_2$ . Lane 1, Gene ruler 1 kb DNA ladder; Lane 2, DNA alone; Lane 3,  $\text{H}_2\text{O}_2$  alone; Lane 4, DNA+6.5 mM Zn(2-pc)+2 mM  $\text{H}_2\text{O}_2$ ; Lane 5–10, involve DNA+2 mM  $\text{H}_2\text{O}_2$ +6.5 mM Co(2-pc) in the presence of various scavengers: Lane 5, 2 mM DMSO; Lane 6, 2 mM D-Mannitol; Lane 7, 2 mM t-butanol; Lane 8, 2 mM KI; Lane 9, 1 mM  $\text{NaN}_3$ ; Lane 10, 1.5 mM  $\text{NaN}_3$ .      96
- Figure 3.7.1      IR spectrum of Co(mal)      100



Figure 3.7.2	IR spectrum of Zn(mal)	100
Figure 3.7.3	IR spectrum of malonic acid	101
Figure 3.7.4	IR spectrum of sodium malonate	101
Figure 3.7.5	UV-Vis spectrum of Co(mal)	104
Figure 3.7.6	UV-Vis spectrum of Zn(mal)	104
Figure 3.7.7	Voltammogram of Co(mal)	105
Figure 3.7.8	Voltammogram of Zn(mal)	106
Figure 3.7.9	TGA of Co(mal)	107
Figure 3.7.10	The postulated decomposition of Co(mal)	109
Figure 3.7.11	TGA of Zn(mal)	109
Figure 3.7.12	The postulated decomposition of Zn(mal)	111
Figure 3.7.13	Postulated structure of diaquabis(malonato)cobalt(II), [Co(mal)] (Wang <i>et al.</i> ,2005)	112
Figure 3.7.14	Postulated structure of diaquabis(malonato)zinc(II), [Zn(mal)] (Ray <i>et al.</i> , 1982)	112

Figure 3.8.1 Agarose (1%) gel electrophoresis banding patterns 114  
of plasmid pBR322 ( $0.025 \mu\text{g}\mu\text{L}^{-1}$ ) treated with various concentration of Co(mal) in the presence of 2 mM  $\text{H}_2\text{O}_2$  and Tris-HCl buffer pH 4.5. Lane 1, Gene ruler 1 kb DNA ladder; Lane 2, DNA alone; Lane 3,  $\text{H}_2\text{O}_2$  alone; Lane 4, DNA+5.8 mM Co(mal); Lane 5–12 involve DNA+2 mM  $\text{H}_2\text{O}_2$ +different concentration of Co(mal): Lane 5, 5.3 mM; Lane 6, 5.4 mM; Lane 7, 5.5 mM; Lane 8, 5.4 mM; Lane 9, 5.5 mM; Lane 10, 5.6 mM; Lane 11, 5.7 mM; Lane 12, 5.8 mM.

Figure 3.8.2 Agarose (1%) gel electrophoresis banding patterns 115  
of plasmid pBR322 ( $0.025 \mu\text{g}\mu\text{L}^{-1}$ ) treated with various concentration of Zn(mal) in the presence of 2 mM  $\text{H}_2\text{O}_2$  and Tris-HCl buffer pH 4.5. Lane 1, Gene ruler 1 kb DNA ladder; Lane 2, DNA alone; Lane 3,  $\text{H}_2\text{O}_2$  alone; Lane 4, DNA+10.2 mM Zn(mal); Lane 5–12 involve DNA+2 mM  $\text{H}_2\text{O}_2$ +different concentration of Zn(mal): Lane 5, 9.5 mM; Lane 6, 9.6 mM; Lane 7, 9.7 mM; Lane 8, 9.8 mM; Lane 9, 9.9 mM; Lane 10, 10.0 mM; Lane 11, 10.1 mM; Lane 12, 10.2 mM.

- Figure 3.8.3      Effect of hydroxyl radicals scavengers and singlet oxygen scavengers on the DNA cleavage of pBR322 ( $0.025 \mu\text{g}\mu\text{L}^{-1}$ ) by 5.5 mM of Co(mal) in the presence of 2 mM  $\text{H}_2\text{O}_2$ . Lane 1, Gene ruler 1 kb DNA ladder; Lane 2, DNA alone; Lane 3,  $\text{H}_2\text{O}_2$  alone; Lane 4, DNA+5.5 mM Co(mal)+2 mM  $\text{H}_2\text{O}_2$ ; Lane 5–10, involve DNA+2 mM  $\text{H}_2\text{O}_2$ +5.5 mM Co(mal) in the presence of various scavengers: Lane 5, 2 mM DMSO; Lane 6, 2 mM D-Mannitol; Lane 7, 2 mM t-butanol; Lane 8, 2 mM KI; Lane 9, 1 mM  $\text{NaN}_3$ ; Lane 10, 1.5 mM  $\text{NaN}_3$ .      116
- Figure 3.8.4      Effect of hydroxyl radicals scavengers and singlet oxygen scavengers on the DNA cleavage of pBR322 ( $0.025 \mu\text{g}\mu\text{L}^{-1}$ ) by 9.8 mM of Zn(mal) in the presence of 2 mM  $\text{H}_2\text{O}_2$ . Lane 1, Gene ruler 1 kb DNA ladder; Lane 2, DNA alone; Lane 3,  $\text{H}_2\text{O}_2$  alone; Lane 4, DNA+9.8 mM Zn(mal)+2 mM  $\text{H}_2\text{O}_2$ ; Lane 5–10, involve DNA+2 mM  $\text{H}_2\text{O}_2$ +9.8 mM Zn(mal) in the presence of various scavengers: Lane 5, 2 mM DMSO; Lane 6, 2 mM D-Mannitol; Lane 7, 2 mM t-butanol; Lane 8, 2 mM KI; Lane 9, 1 mM  $\text{NaN}_3$ ; Lane 10, 1.5 mM  $\text{NaN}_3$ .      117
- Figure 3.9.1      IR spectrum of Co(gly)      122

Figure 3.9.2	IR spectrum of glycine	122
Figure 3.9.3	IR spectrum of sodium glycinate	123
Figure 3.9.4	IR spectrum of Co(glycol)	124
Figure 3.9.5	IR spectrum of glycolic acid	124
Figure 3.9.6	IR spectrum of sodium glycolate	125
Figure 3.9.7	IR spectrum of Co(3,5-dn)	126
Figure 3.9.8	IR spectrum of 3,5-dinitrobenzoic acid	126
Figure 3.9.9	IR spectrum of sodium 3,5-dinitrobenzate	127
Figure 3.9.10	IR spectrum of Co(quino)	128
Figure 3.9.11	IR spectrum of quinolinic acid	128
Figure 3.9.12	IR spectrum of sodium quinolate	129
Figure 3.9.13	IR of Co(pyd-2,5-dc)	130
Figure 3.9.14	IR spectrum of 2,5-dinitrobenzoic acid	130
Figure 3.9.15	IR spectrum of sodium 2,5-dinitrobenzoate	131
Figure 3.9.16	IR spectrum of Co(4-amino)	132
Figure 3.9.17	IR spectrum of 4-aminobenzoic acid	132
Figure 3.9.18	IR spectrum of sodium 4-aminobenzate	133
Figure 3.9.19	UV-Vis spectrum of Co(gly)	136
Figure 3.9.20	UV-Vis spectrum of Co(glycol)	137
Figure 3.9.21	UV-Vis spectrum of Co(3,5-dn)	137
Figure 3.9.22	UV-Vis spectrum of Co(quino)	138
Figure 3.9.23	UV-Vis spectrum of Co(pyd-2,5-dc)	138
Figure 3.9.24	UV-Vis spectrum of Co(4-amino)	139
Figure 3.9.25	Voltammogram of Co(gly)	140
Figure 3.9.26	Voltammogram of Co(glycol)	140

Figure 3.9.27	Voltammogram of Co(3,5-dn)	141
Figure 3.9.28	Voltammogram of Co(quino)	141
Figure 3.9.29	Voltammogram of Co(pyd-2,5-dc)	142
Figure 3.9.30	Voltammogram of Co(4-amino)	142
Figure 3.9.31	TGA curves of Co(gly)	143
Figure 3.9.32	The postulated decomposition diagram of Co(gly)	145
Figure 3.9.33	TGA curves of Co(glycol)	146
Figure 3.9.34	The decomposition diagram of Co(glycol)	148
Figure 3.9.35	TGA curves of Co(3,5-dn)	149
Figure 3.9.36	The postulated decomposition diagram of Co(3,5-dn)	151
Figure 3.9.37	TGA curves of Co(quino)	152
Figure 3.9.38	The postulated decomposition diagram of Co(quino)	154
Figure 3.9.39	TGA curves of Co(pyd-2,5-dc)	155
Figure 3.9.40	The postulated decomposition diagram of Co(pyd-2,5-dc)	157
Figure 3.9.41	TGA curves of Co(4-amino)	158
Figure 3.9.42	The postulated decomposition diagram of Co(4-amino)	160
Figure 3.9.43	Postulated structure of diaquadichloro(glycine)cobalt(II), [Co(gly)] (Clegg <i>et al.</i> , 1987)	161

Figure 3.9.44	Molecular structure of diaquadichloro(glycine)cobalt(II), [Co(gly)] (Clegg <i>et al.</i> , 1987)	161
Figure 3.9.45	Postulated structure of bis(glycolato)cobalt(II), [Co(glycol)] (Medina <i>et al.</i> , 2000)	162
Figure 3.9.46	Molecular structure of polymeric bis(glycolato)cobalt(II), [Co(glycol)] (Medina <i>et al.</i> , 2000)	162
Figure 3.9.47	Postulated structure of tetraaquabis(3,5-dinitrobenzoato- <i>O</i> )cobalt(II)tetrahydrate, [Co(3,5-dn)] (Tahir <i>et al.</i> , 1996)	163
Figure 3.9.48	Postulated structure of diaqua(pyridine-2,3-dicarboxylato)cobalt(II), [Co(quino)] (Zhang <i>et al.</i> , 2003)	164
Figure 3.9.49	The molecular structure of diaqua(pyridine-2,3-dicarboxylato)cobalt(II), [Co(quino)] (Zhang <i>et al.</i> , 2003)	164
Figure 3.9.50	Postulated structure of diaquabis(pyridine-2,5-dicarboxylato)cobalt(II), [Co(pyd-2,5-dc)] (Xu <i>et al.</i> , 2004)	165
Figure 3.9.51	Postulated structure of diaquabis(4-aminobenzoato)cobalt(II), [Co(4-amino)] (Amiraslanov <i>et al.</i> , 1978)	165

Figure 3.9.52	The molecular structure of diaquabis(4-aminobenzoato)cobalt(II), [Co(4-amino)] (Amiraslanov <i>et al.</i> , 1978)	166
Figure 3.10.1	Agarose (1%) gel electrophoresis banding patterns of plasmid pBR322 ( $0.025 \mu\text{g}\mu\text{L}^{-1}$ ) treated with various concentration of Co(gly) in the presence of 2 mM $\text{H}_2\text{O}_2$ and Tris-HCl buffer pH 4.5. Lane 1, Gene ruler 1 kb DNA ladder; Lane 2, DNA alone; Lane 3, $\text{H}_2\text{O}_2$ alone; Lane 4, DNA+4.1 mM Co(gly); Lane 5–12 involve DNA+2 mM $\text{H}_2\text{O}_2$ +different concentration of Co(gly): Lane 5, 3.4 mM; Lane 6, 3.5 mM; Lane 7, 3.6 mM; Lane 8, 3.7 mM; Lane 9, 3.8 mM; Lane 10, 3.9 mM; Lane 11, 4.0 mM; Lane 12, 4.1 mM.	168

Figure 3.10.2 Agarose (1%) gel electrophoresis banding patterns of plasmid pBR322 ( $0.025 \mu\text{g}\mu\text{L}^{-1}$ ) treated with various concentration of Co(glycol) in the presence of 2 mM  $\text{H}_2\text{O}_2$  and Tris-HCl buffer pH 4.5. Lane 1, Gene ruler 1 kb DNA ladder; Lane 2, DNA alone; Lane 3,  $\text{H}_2\text{O}_2$  alone; Lane 4, DNA+4.4 mM Co(glycol); Lane 5–12 involve DNA+2 mM  $\text{H}_2\text{O}_2$ +different concentration of Co(glycol): Lane 5, 3.7 mM; Lane 6, 3.8 mM; Lane 7, 3.9 mM; Lane 8, 4.0 mM; Lane 9, 4.1 mM; Lane 10, 4.2 mM; Lane 11, 4.3 mM; Lane 12, 4.4 mM.

Figure 3.10.3 Agarose (1%) gel electrophoresis banding patterns of plasmid pBR322 ( $0.025 \mu\text{g}\mu\text{L}^{-1}$ ) treated with various concentration of Co(3,5-dn) in the presence of 2 mM  $\text{H}_2\text{O}_2$  and Tris-HCl buffer pH 4.5. Lane 1, Gene ruler 1 kb DNA ladder; Lane 2, DNA alone; Lane 3,  $\text{H}_2\text{O}_2$  alone; Lane 4, DNA+1.9 mM Co(3,5-dn); Lane 5–12 involve DNA+2 mM  $\text{H}_2\text{O}_2$ +different concentration of Co(3,5-dn): Lane 5, 1.2 mM; Lane 6, 1.3 mM; Lane 7, 1.4 mM; Lane 8, 1.5 mM; Lane 9, 1.6 mM; Lane 10, 1.7 mM; Lane 11, 1.8 mM; Lane 12, 1.9 mM.



Figure 3.10.4 Agarose (1%) gel electrophoresis banding patterns of plasmid pBR322 ( $0.025 \mu\text{g}\mu\text{L}^{-1}$ ) treated with various concentration of Co(quino) in the presence of 2 mM  $\text{H}_2\text{O}_2$  and Tris-HCl buffer pH 4.5. Lane 1, Gene ruler 1 kb DNA ladder; Lane 2, DNA alone; Lane 3,  $\text{H}_2\text{O}_2$  alone; Lane 4, DNA+1.7 mM Co(quino); Lane 5–12 involve DNA+2 mM  $\text{H}_2\text{O}_2$ +different concentration of Co(quino): Lane 5, 1.0 mM; Lane 6, 1.1 mM; Lane 7, 1.2 mM; Lane 8, 1.3 mM; Lane 9, 1.4 mM; Lane 10, 1.5 mM; Lane 11, 1.6 mM; Lane 12, 1.7 mM. 171

Figure 3.10.5 Agarose (1%) gel electrophoresis banding patterns of plasmid pBR322 ( $0.025 \mu\text{g}\mu\text{L}^{-1}$ ) treated with various concentration of Co(pyd-2,5-dc) in the presence of 2 mM  $\text{H}_2\text{O}_2$  and Tris-HCl buffer pH 4.5. Lane 1, Gene ruler 1 kb DNA ladder; Lane 2, DNA alone; Lane 3,  $\text{H}_2\text{O}_2$  alone; Lane 4, DNA+1.1 mM Co(pyd-2,5-dc); Lane 5–12 involve DNA+2mM  $\text{H}_2\text{O}_2$ +different concentration of Co(pyd-2,5-dc): Lane 5, 0.4 mM; Lane 6, 0.5 mM; Lane 7, 0.6 mM; Lane 8, 0.7 mM; Lane 9, 0.8 mM; Lane 10, 0.9 mM; Lane 11, 1.0 mM; Lane 12, 1.1 mM. 172

Figure 3.10.6 Agarose (1%) gel electrophoresis banding patterns of plasmid pBR322 ( $0.025 \mu\text{g}\mu\text{L}^{-1}$ ) treated with various concentration of Co(4-amino) in the presence of 2 mM  $\text{H}_2\text{O}_2$  and Tris-HCl buffer pH 4.5. Lane 1, Gene ruler 1 kb DNA ladder; Lane 2, DNA alone; Lane 3,  $\text{H}_2\text{O}_2$  alone; Lane 4, DNA+2.9 mM Co(4-amino); Lane 5–12 involve DNA+2 mM  $\text{H}_2\text{O}_2$ +different concentration of Co(4-amino): Lane 5, 2.2 mM; Lane 6, 2.3 mM; Lane 7, 2.4 mM; Lane 8, 2.5 mM; Lane 9, 2.6 mM; Lane 10, 2.7 mM; Lane 11, 2.8 mM; Lane 12, 2.9 mM.

Figure 3.10.7 Effect of hydroxyl radicals scavengers and singlet oxygen scavengers on the DNA cleavage of pBR322 ( $0.025 \mu\text{g}\mu\text{L}^{-1}$ ) by 3.9 mM of Co(gly) in the presence of 2 mM  $\text{H}_2\text{O}_2$ . Lane 1, Gene ruler 1 kb DNA ladder; Lane 2, DNA alone; Lane 3,  $\text{H}_2\text{O}_2$  alone; Lane 4, DNA+3.9 mM Co(gly)+2 mM  $\text{H}_2\text{O}_2$ ; Lane 5–10, involve DNA+2 mM  $\text{H}_2\text{O}_2$ +3.9 mM Co(gly) in the presence of various scavengers: Lane 5, 2 mM DMSO; Lane 6, 2 mM D-Mannitol; Lane 7, 2 mM t-butanol; Lane 8, 2 mM KI; Lane 9, 1 mM  $\text{NaN}_3$ ; Lane 10, 1.5 mM  $\text{NaN}_3$ .

Figure 3.10.8      Effect of hydroxyl radicals scavengers and singlet oxygen scavengers on the DNA cleavage of pBR322 ( $0.025 \mu\text{g}\mu\text{L}^{-1}$ ) by 3.9 mM of Co(glycol) in the presence of 2 mM  $\text{H}_2\text{O}_2$ . Lane 1, Gene ruler 1 kb DNA ladder; Lane 2, DNA alone; Lane 3,  $\text{H}_2\text{O}_2$  alone; Lane 4, DNA+3.9 mM Co(glycol)+2 mM  $\text{H}_2\text{O}_2$ ; Lane 5–10, involve DNA+2 mM  $\text{H}_2\text{O}_2$ +3.9 mM Co(glycol) in the presence of various scavengers: Lane 5, 2 mM DMSO; Lane 6, 2 mM D-Mannitol; Lane 7, 2 mM t-butanol; Lane 8, 2 mM KI; Lane 9, 1 mM  $\text{NaN}_3$ ; Lane 10, 1.5 mM  $\text{NaN}_3$ .      175

Figure 3.10.9      Effect of hydroxyl radicals scavengers and singlet oxygen scavengers on the DNA cleavage of pBR322 ( $0.025 \mu\text{g}\mu\text{L}^{-1}$ ) by 1.7 mM of Co(3,5-dn) in the presence of 2 mM  $\text{H}_2\text{O}_2$ . Lane 1, Gene ruler 1 kb DNA ladder; Lane 2, DNA alone; Lane 3,  $\text{H}_2\text{O}_2$  alone; Lane 4, DNA+ 1.7mM Co(3,5-dn)+2 mM  $\text{H}_2\text{O}_2$ ; Lane 5–10, involve DNA+2 mM  $\text{H}_2\text{O}_2$ +1.7 mM Co(3,5-dn) in the presence of various scavengers: Lane 5, 2 mM DMSO; Lane 6, 2 mM D-Mannitol; Lane 7, 2 mM t-butanol; Lane 8, 2 mM KI; Lane 9, 1 mM  $\text{NaN}_3$ ; Lane 10, 1.5 mM  $\text{NaN}_3$ .      176

Figure 3.10.10      Effect of hydroxyl radicals scavengers and singlet oxygen scavengers on the DNA cleavage of pBR322 ( $0.025 \mu\text{g}\mu\text{L}^{-1}$ ) by 1.3 mM of Co(quino) in the presence of 2 mM  $\text{H}_2\text{O}_2$ . Lane 1, Gene ruler 1 kb DNA ladder; Lane 2, DNA alone; Lane 3,  $\text{H}_2\text{O}_2$  alone; Lane 4, DNA+1.3 mM Co(quino)+2 mM  $\text{H}_2\text{O}_2$ ; Lane 5–10, involve DNA+2 mM  $\text{H}_2\text{O}_2$ +1.3 mM Co(quino) in the presence of various scavengers: Lane 5, 2 mM DMSO; Lane 6, 2 mM D-Mannitol; Lane 7, 2 mM t-butanol; Lane 8, 2 mM KI; Lane 9, 1 mM  $\text{NaN}_3$ ; Lane 10, 1.5 mM  $\text{NaN}_3$ .

Figure 3.10.11      Effect of hydroxyl radicals scavengers and singlet oxygen scavengers on the DNA cleavage of pBR322 ( $0.025 \mu\text{g}\mu\text{L}^{-1}$ ) by 0.9 mM of Co(pyd-2,5-dc) in the presence of 2 mM  $\text{H}_2\text{O}_2$ . Lane 1, Gene ruler 1 kb DNA ladder; Lane 2, DNA alone; Lane 3,  $\text{H}_2\text{O}_2$  alone; Lane 4, DNA+0.9 mM Co(pyd-2,5-dc)+2 mM  $\text{H}_2\text{O}_2$ ; Lane 5–10, involve DNA+2 mM  $\text{H}_2\text{O}_2$ +0.9 mM Co(pyd-2,5-dc) in the presence of various scavengers: Lane 5, 2 mM DMSO; Lane 6, 2 mM D-Mannitol; Lane 7, 2 mM t-butanol; Lane 8, 2 mM KI; Lane 9, 1 mM  $\text{NaN}_3$ ; Lane 10, 1.5 mM  $\text{NaN}_3$ .

Figure 3.10.12      Effect of hydroxyl radicals scavengers and singlet oxygen scavengers on the DNA cleavage of pBR322 ( $0.025 \mu\text{g}\mu\text{L}^{-1}$ ) by 2.4 mM of Co(4-amino) in the presence of 2 mM  $\text{H}_2\text{O}_2$ . Lane 1, Gene ruler 1 kb DNA ladder; Lane 2, DNA alone; Lane 3,  $\text{H}_2\text{O}_2$  alone; Lane 4, DNA+2.4 mM Co(4-amino)+2 mM  $\text{H}_2\text{O}_2$ ; Lane 5–10, involve DNA+2 mM  $\text{H}_2\text{O}_2$ +2.4 mM Co(4-amino) in the presence of various scavengers: Lane 5, 2 mM DMSO; Lane 6, 2 mM D-Mannitol; Lane 7, 2 mM t-butanol; Lane 8, 2 mM KI; Lane 9, 1 mM  $\text{NaN}_3$ ; Lane 10, 1.5 mM  $\text{NaN}_3$ .

# SINTESIS, PENCIRIAN DAN DAYA PEMBELAHAN DNA KOMPLEKS KOBALT(II) DAN KOMPLEKS ZINK(II)

## ABSTRAK

Sebanyak sepuluh kompleks kobalt(II) dan empat kompleks zink(II) telah berjaya disintesis daripada tindak balas antara kobalt(II)klorida heksahidrat,  $\text{CoCl}_2 \cdot 6\text{H}_2\text{O}$  atau zink(II)asetat dihidrat,  $\text{Zn}(\text{CH}_3\text{COO})_2 \cdot 2\text{H}_2\text{O}$  dengan ligan asid karboksilik. Lapan kompleks yang mempunyai isostruktur yang sama telah disintesis antara  $\text{CoCl}_2 \cdot 6\text{H}_2\text{O}$  atau  $\text{Zn}(\text{CH}_3\text{COO})_2 \cdot 2\text{H}_2\text{O}$  dengan ligan asid pirazina-2-karboksilik, asid maleik, asid 2-pikolinik dan asid malonik. Seterusnya, enam kompleks yang lain telah disintesis melalui  $\text{CoCl}_2 \cdot 6\text{H}_2\text{O}$  dengan ligan glisina, asid glikolik, asid 3,5-dinitrobenzoik, asid quinolinik, asid piridina-2,5-dikarboksilik dan asid 4-aminobenzoik. Kompleks yang telah disintesis ini dicirikan melalui pelbagai kaedah fizik seperti penentuan takat lebur, konduktiviti, Spektroskopi Inframerah (FT-IR), Mikroanalisis CHN, Spektroskopi Penyerapan Atom (AAS), Spektroskopi Ultralembayung (UV-Vis), Voltametri Siklik (CV), Analisis Termogravimetrik (TGA) dan X-ray Kristalografi. Manakala sifat biologi kompleks ini telah dianalisis melalui Pemetongan Plasmid DNA dan Pengasaian MTT. Melalui analisis Spektroskopi Inframerah, didapati bahawa kesemua 14 kompleks ini menunjukkan ligan terikat secara monodentat kepada pusat atom Co(II) atau Zn(II). Manakala, analisis UV-Vis menunjukkan bahawa keadaan pengoksidaan bagi atom kobalt dalam kompleks ialah +2 dan mempunyai konfigurasi  $d^7$  dan kompleks zink juga dalam keadaan pengoksidaan + 2 tetapi dengan konfigurasi  $d^{10}$ . Keupayaan sifat redoks di dalam kompleks adalah amat perlu untuk kegunaan biologi dan ini dapat

ditentukan melalui analisis CV. Hasil kajian eksperimen pemotongan plasmid DNA menunjukkan kesemua kompleks berupaya memotong plasmid DNA dimana pemotongan tersebut menghasilkan jaluran tunggal serta jaluran berganda DNA. Keberkesanan pemotongan plasmid DNA ini bergantung secara langsung dengan kepekatan kompleks. Kompleks kobalt(II) menunjukkan pemotongan plasmid yang lebih baik berbanding dengan kompleks zink(II). Selain itu, kompleks kobalt(II) juga memberikan keputusan aktiviti sitotoksik yang lebih baik berbanding dengan kompleks zink(II) dalam eksperimen pengasaan MTT.

# SYNTHESIS, CHARACTERIZATION AND DNA CLEAVAGE ABILITY OF COBALT(II) COMPLEXES AND ZINC(II) COMPLEXES

## ABSTRACT

A total of ten cobalt(II) complexes and four zinc(II) complexes had been successfully synthesized between the reaction of cobalt(II)chloride hexahydrate,  $\text{CoCl}_2 \cdot 6\text{H}_2\text{O}$  or zinc(II)acetate dihydrate,  $\text{Zn}(\text{CH}_3\text{COO})_2 \cdot 2\text{H}_2\text{O}$  with carboxylic acids. Eight isostructural of complexes Co(II) and Zn(II) were formed by the reaction of  $\text{CoCl}_2 \cdot 6\text{H}_2\text{O}$  or  $\text{Zn}(\text{CH}_3\text{COO})_2 \cdot 2\text{H}_2\text{O}$  with pyrazine-2-carboxylic acid, maleic acid, 2-picolinic acid and malonic acid while the others six complexes were synthesized by the reaction of  $\text{CoCl}_2 \cdot 6\text{H}_2\text{O}$  with glycine, glycolic acid, 3,5-dinitrobenzoic acid, quinolinic acid, pyridine-2,5-dicarboxylic acid and 4-aminobenzoic acid. These complexes were characterized by determination of melting point, conductivity measurement, Fourier Transform Infrared Spectroscopy (FT-IR), microanalysis CHN, Atomic Absorption Spectroscopy (AAS), Cyclic Voltammetry (CV), Thermogravimetry Analysis (TGA) and X-ray Crystallography. While the biological properties of these complexes were determined by DNA Cleavage and MTT Assay. From the FT-IR analysis, all the ligands coordinated the atoms Co(II) and Zn(II) in monodentate. While from UV-Vis analysis, the oxidation state of the cobalt(II) complexes were in +2 and showed d-d transition peaks corresponding to  $d^7$  system while the oxidation state of zinc(II) complexes were also +2 and in  $d^{10}$  system. The CV analysis showed that all these complexes have the reversible redox ability which is very important in the biological uses. Gel electrophoresis experiments showed that all the complexes successfully promoted the cleavage of



plasmid DNA by producing single or double DNA strand breaks. All the cobalt(II) complexes were shown better in biological properties compared to zinc(II) complexes whether in DNA cleavage or MTT Assay.

# CHAPTER 1

## INTRODUCTION

### 1.1 DNA

Deoxyribonucleic acid (DNA) is a nucleic acid that contains the genetic instructions used in the development and functioning of all known living organisms and some viruses (Figure 1.1).

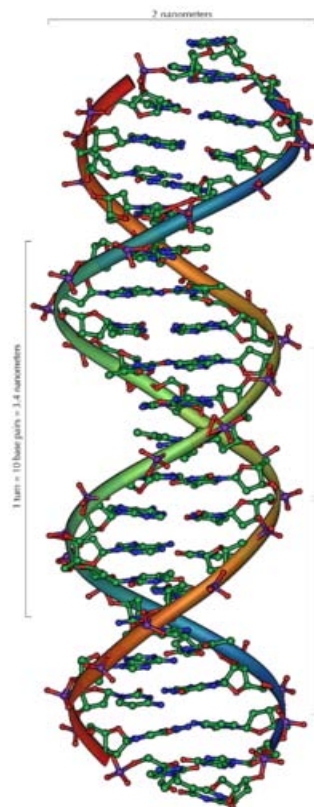


Figure 1.1 Double helix DNA

The main role of DNA molecules is the long-term storage of information. DNA is often compared to a set of blueprints or a recipe, since it contains the

instructions needed to construct other components of cells, such as proteins and RNA molecules. The DNA segments that carry this genetic information are called genes, but other DNA sequences have structural purposes, or are involved in regulating the use of this genetic information.

Chemically, DNA consists of two long polymers of simple units called nucleotides, with backbones made of sugars and phosphate groups joined by ester bonds. These two strands run in opposite directions to each other and are therefore anti-parallel. Attached to each sugar is one of four types of molecules called bases (adenine, thymine, guanine and cytosine) (Figure 1.2).

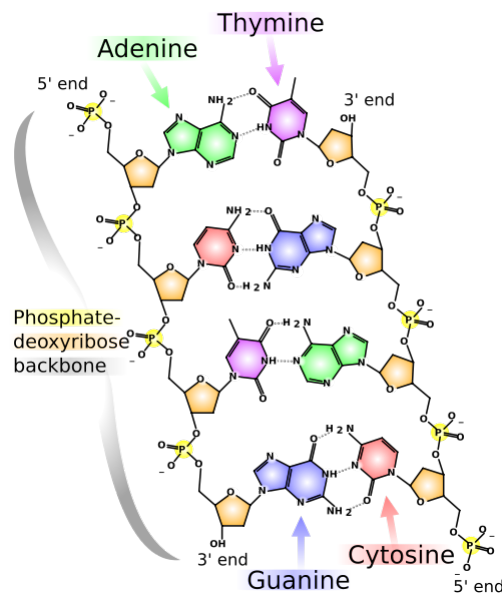


Figure 1.2 The chemical structure of DNA

It is the sequence of these four bases along the backbone that encodes information. This information is read using the genetic code, which specifies the sequence of the amino acids within proteins. The code is read by copying stretches of DNA into the nucleic acid RNA, in a process called transcription.

Within cells, DNA is organized into structures called chromosomes. These chromosomes are duplicated before cells divide, in a process called DNA replication. Eukaryotic organisms (animals, plants, fungi, and protists) store their DNA inside the cell nucleus, while in prokaryotes (bacteria and archae) it is found in the cell's cytoplasm. Within the chromosomes, chromatin proteins such as histones compact and organize DNA. These compact structures guide the interactions between DNA and other proteins, helping control which parts of the DNA are transcribed.

### 1.2 Metals used as DNA cleaving agents

According to the American Cancer Society, cancer is the second leading cause of death in the United States. For this reason, over the past 40 years, there has been a vast interest in development of efficient anticancer drugs that possess minimal side effects. Cancer is a class of disease in which there is uncontrolled cell division. Malignant tumor cells spread directly into the adjacent tissue or indirectly by metastasis. Therefore, the interaction of transition metal complexes with DNA has been extensively studied in the past few decades. Beginning in the early 1980's, researchers began examining the interactions of coordinated complexes of cobalt, zinc, copper, nickel, iron, chromium, rhodium, osmium and ruthenium. DNA-interactions of many transition metal compounds containing intercalative ligands such as 1,10-phenanthroline and substituted phenanthrolines had been investigated. Metal complexes are a particularly attractive species to recognize and cleave DNA. The ligands or the metal in these complexes can be varied in an easily controlled manner to facilitate an individual application. The change in metal ion or ligand

leads to changes in the binding mode and affinity. Transition metal complexes can interact non-covalently with DNA by intercalation, groove binding, or external electrostatic binding. Among the factors governing the binding modes, it appears that the most significant is the molecular shape. Those complexes that best fit against the DNA helical structure display the highest binding affinity. Many useful applications of these complexes require that the complex bind to DNA through an intercalative mode with the ligand intercalating into the adjacent base pairs of DNA. When the size, shape and chirality of the complexes fit the DNA structure, the complexes may approach closely to and intercalate into the base pairs of DNA. On the other hand, upon irradiation, these complexes can induce the single or double-stranded cleavage of plasmid DNA. Although the interactions of the complexes with DNA have been investigated extensively, the knowledge of the nature of binding of some complexes and their binding geometries has remained relatively modest.

One of the usage of transition metal complexes is anticancer agents. Disruption of DNA synthesis in cancerous cells is carried out by transition metal complexes in a variety of ways. For example, titanium uses the glycoprotein transferrin to enter the cell, gold is highly cytotoxic, attacking the mitochondria but it also attacking healthy cells, estrogen-derived steroidal metal complexes access the cells by binding to estrogen receptors. Palladium acts by disruption of the double helix in the DNA leaving most of the base pairs intact indicating that the complex does not insert itself into the sequence.

The first transition metal successfully used as an anticancer agent was platinum. It was used in a compound called cisplatin (Figure 1.3) (Rosenberg *et al.*, 1969; Rosenberg *et al.*, 1970).

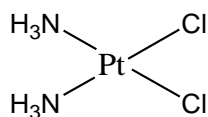


Figure 1.3 Cisplatin

Platinum complexes form interstrand and intrastrand adducts depending on the number of metal centres. This enables high mobility group (HMG1) proteins to recognize damaged DNA (Cox *et al*, 2001). It also reacts with neighboring purine residues (adjacent intrastand guanines and adenines) to form intrastand adducts in DNA (Sullivan *et al*, 2000). So, it has the ability to inhibit tumors and is widely used alone or in combination with other chemotherapeutic drugs for the treatment of several aggressive cancers like solid malignant tumors such as those found in the head and neck, lungs, ovary, bladder and testicles (Abrams and Messer, 1993; Weiss and Christian, 1993). Although treatment with cisplatin is often effective, serious side-effects such as nausea, nephrotoxicity, neurotoxicity and ototoxicity often occur (Reedijk, 1996). In addition, cisplatin, which is administered intravenously, has limited solubility in aqueous solution (Wong and Giandomenico, 1999). This has led to intensive efforts in developing newer platinum drugs that show similar efficiency to cisplatin but exhibit less toxicity.

### 1.3 Usage and application of cobalt complexes

Cobalt has both beneficial and harmful effects on humans. Cobalt is an essential element for humans since it is part of vitamin B12. The amount needed is very small, and the body contains only about 1 milligram. It may be used in the

treatment of anemia. Exposure to cobalt may cause lung effects, which include respiratory irritation, coughing, asthma, pulmonary oedema, and pneumonia. The International Agency for Research on Cancer classifies cobalt as a 'possible human carcinogen'. Exposure to cobalt salts may cause skin problems, and may damage the kidneys and cause lung damage. Cobalt can also damage the heart, causing heart failure. Repeated exposure can cause scarring of the lungs (pulmonary fibrosis) which may not be noticed without a chest x - ray. This can be disabling or fatal.

The largest use of cobalt metal is to make alloys, which retain strength even when very hot. It is also used to help paint dry quickly. Cobalt is also used to make artificial body parts such as hip and knee joints. Cobalt carbonate is used in ceramics and as an animal feed supplement in trace amounts. Cobalt chloride is used as a humidity and water indicator, in electroplating, in the manufacture of vitamin B-12, as a fertilizer and feed additive in trace amounts. Cobalt oxide is used in pigments for ceramics and glass, in fast drying paints and varnishes, in semiconductors, in enamel coatings on steel, and again as an animal feed additive in trace amounts. Cobalt sulfate is used in electroplating, in batteries, as a drying agent in inks and varnishes, in enamels, and ceramics, and as a feed and fertilizer additive.

#### 1.4 Cobalt in antitumor complexes

*Mer-tris*( $\beta$ -alaninato)cobalt(III), *mer*-[Co( $\beta$ -ala)<sub>3</sub>] alone does not cleave DNA but can do so in the presence of ascorbic acid in TBE buffer pH 8.3. DNA cleavage can be attributed to ascorbate free radicals generated by one-electron transfer from ascorbate ions to *mer*-[Co( $\beta$ -ala)<sub>3</sub>]. The nucleolytic ability of *mer*-[Co( $\beta$ -ala)<sub>3</sub>] in the

presence of ascorbic acid results from the reduction of the complex by ascorbic acid. Using MTT assay, preliminary studies revealed anti-cancer properties of  $\text{CoCl}_2$  ( $\text{IC}_{50}=0.06$  mM),  $\text{mer-}[\text{Co}(\beta\text{-ala})_3]$  ( $\text{IC}_{50}=2.06$  mM) and  $\{\text{mer-}[\text{Co}(\beta\text{-ala})_3]+0.20$  mM  $\text{H}_2\text{A}$  system} ( $\text{IC}_{50}=1.61$  mM) towards lung cancer cell line PC9 (Ng *et al*, 2005).

Bis(phenanthrenequinoato)cobalt have been synthesized and tested on the human breast cancer cell line T47D rich in progesterone receptors and the  $\text{IC}_{50}$  value is  $2.04$   $\mu\text{M}$  (Afrasiabi *et al*, 2003). It is clearly observed that complexation with metals has a synergetic effect on the antiproliferative activity. Under certain conditions, a number of metals have been observed to inhibit steroid binding to the cognate receptors or prevent dimerization of the estrogen receptors, due perhaps to the involvement of the thiols in steroid binding.

Generally, cobalt (II) and cobalt (III) complexes show antitumor activities *in vivo*. Hence, recently the interaction of cobalt complexes with DNA has attracted much attention. In a report, Shimakoshi *et al.*, 2003 have shown that a dicobalt complex was more efficient in cleaving DNA compared to an equivalent monomeric complex. Synthesis of new cobalt (II) and cobalt (III) complexes enabled chemists to extensively study the ability of these complexes to act as probes in investigating the structure of DNA. One compound is  $\text{cis-}[\text{Co}(\text{phen})_2(\text{BPEI})\text{Cl}]\text{Cl}_2\cdot 4\text{H}_2\text{O}$  (phen=1,10-phenanthroline, BPEI=branched polyethyleneimine) (Shimakoshi *et al*, 2003). Preliminary results from the absorption and fluorescence spectral studies show that the polymer-cobalt(III) complex with high cobalt(III) chelate content binds strongly to DNA. Binding of this complex with DNA was also studied by gel electrophoresis using plasmid pBR 322 DNA. This DNA moves on agarose gel under the influence of an electrical field. This movement is retarded when the DNA are bound to other molecules. Many polycationic polymeric molecules interact with DNA through



electrostatic interactions between phosphate groups of the DNA and oppositely charged groups of polymer. The gel retardation assay performed on pBR322 DNA demonstrates that the cationic segments of the polyethyleneimine might have neutralized the negative charges of DNA which could have facilitated further due to the increased intercalation of the planar phen groups of cobalt(III) complex moieties. The IC<sub>50</sub> value of the complex was higher for the 24 h treatment groups, i.e., in the range of 100–140 µg/mL, whereas for the 48 h treatment groups the IC<sub>50</sub> value fell in the range of 45–65 µg/mL.

### 1.5 Usage and application of zinc complexes

Zinc is also an essential metal for human health. It is vital for many biological functions such as disease resistance, wound healing, digestion, reproduction, physical growth, diabetes control, taste and smell. It is estimated that 3000 of the hundreds of thousands of proteins in the human body contain zinc prosthetic groups. In addition, there are over a dozen types of cells in the human body that secrete zinc ions, and the roles of these secreted zinc signals in medicine and health are now being actively studied. Intriguingly, brain cells in the mammalian forebrain are one type of cell that secretes zinc, along with its other neuronal messenger substances. Cells in the salivary gland, prostate, immune system and intestine are other types that secrete zinc.

Zinc is an activator of certain enzymes, such as carbonic anhydrase. Carbonic anhydrase is important in the transport of carbon dioxide in vertebrate blood. It is

also required in plants for leaf formation, the synthesis of indole acetic acid (auxin) and anaerobic respiration (alcoholic fermentation).

### 1.6 Zinc in antitumor complexes

Zn(phen)(edda) (phen=1,10-phenanthroline, edda=ethylenediaminediacetic acid) complexes was found to have promising antitumor qualities. The gel electrophoresis result shows that the extent of DNA cleavage by the Zn(phen)(edda) complex is dependent on both the concentration. The concentration factor has a limiting effect as no further increase in DNA cleavage occurs beyond the limiting concentration. The IC<sub>50</sub> for this compound is 7.0 µg/mL for incubation time of 72 hours (Seng *et al*, 2008). Tatjana *et al.* showed that the antiproliferative activity of zinc(II) complexes [Zn(AcPipPheF)<sub>2</sub>] and [Zn(OAc)(AcPip-PheF)]<sub>2</sub> where AcPip-PheF is 2-acetyl pyridine 1-(4-fluorophenyl)-piperazinyl thiosemicarbazone was found to be considerably stronger than that of cis-platin. The IC<sub>50</sub> values range from 26 to 90 nM, against all cell lines tested, while for cis-platin the IC<sub>50</sub> values range from 2 to 17 µM and for the zinc salt, ZnCl<sub>2</sub>, the IC<sub>50</sub> values range from 81 to 93 µM (Tatjana *et al*, 2010). Zn(II) complexes [ZnCl<sub>2</sub>(Fo4Npypipe)] and [ZnCl<sub>2</sub>(Ac4Npypipe)] where Fo4Npypipe and Ac4Npypipe are 2-formyl pyridine N(4)-1-(2-pyridyl)-piperazinyl thiosemicarbazone and 2-acetyl pyridine N(4)-1-(2-pyridyl)-piperazinyl thiosemicarbazone respectively considered as agents with potential antitumor activity, and can therefore be candidates for further stages of screening *in vitro* and/or *in vivo* (Dimitra *et al*, 2006).

## 1.7 Mechanism of DNA cleavage

DNA damage is well known to play a critical role in many diseases. Therefore, most metal-based drugs on the market require dioxygen to bring about DNA damage. Even fewer have been shown to induce damage *via* carbon centered radicals. These are the two pathways.

### 1.7.1 Reactive oxygen species (ROS)

The enzyme superoxide dismutase is able to dismutate superoxide anion to form oxygen and hydrogen peroxide. Those ROS have been found to interact directly with DNA or DNA components *via* singlet oxygen species ( $O_2^{\cdot}$ ) and hydroxide radicals ( $\cdot OH$ ). Under aerobic conditions, react with oxygen to produce  $O_2^{\cdot}$  (Heo *et al.*, 2006). However, several works in literature have shown that  $O_2^{\cdot}$  radicals cannot induce DNA damage (Muller and Burrows, 1998). These  $O_2^{\cdot}$  can react with  $H^+$  to generate  $H_2O_2$  which in turn can react with more  $O_2^{\cdot}$  to generate more  $\cdot OH$  *via* Harber-Weiss reactions. The redox potential for  $\cdot OH$  radicals is  $\approx 2.4$  V vs. NHE. Since the redox potential for  $\cdot OH$  is high,  $\cdot OH$  can oxidize DNA, resulting in DNA damage.

ROS induce oxidative stress. *In vivo*, radicals are thought to be produced *via* two main pathways. The first is *via* the exposure of living organisms to ionizing radiation ( $\gamma$  radiolysis) leading to the hemolytic fission of oxygen-hydrogen bonds in water thereby producing an  $\cdot OH$ . The second way is through the generation of  $\cdot OH$  through Fenton reactions. These reactions usually involve a metal ion which acts as a

catalyst in the presence of hydrogen peroxide. The hydrogen peroxide is broken down into a hydrogen ion and a hydroxyl free radical (Figure 1.4).

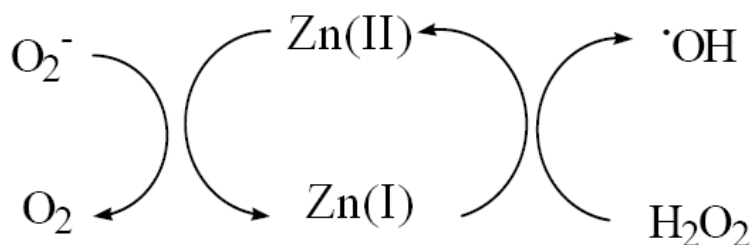


Figure 1.4 Schematic diagram showing metal ion conversion to hydroxyl radicals

It has been shown that DNA  $\cdot OH$  radicals induce DNA damage *via* hydrogen abstraction from the sugar moiety hence forming sugar radicals (Tullius and Pogozelski, 1998). Proven that the major product formed by  $\cdot OH$  DNA damage was 8-OH-Gua suggesting that  $\cdot OH$  radicals are involved in the attack of purine bases (Floyd *et al*, 1986). Three major intermediates that result from  $\cdot OH$  radical attack had been identified. The chemical fates of these intermediates have been extensively studied. Adduct 1 and 2 revert back to guanine by gaining an electron *via* thiols generated in the cells. Adduct 3 (8-OH-Gua) leads to the formation of 7,8-dihydro-8-oxoguanine or can gain an electron and a proton forming 2,6-diamino-5-formamido-4-hydroxypyrimidine (FAPy-G) which eventually leads to DNA damage (Figure 1.5) (Steenken, 1989; O'Neill, 1983).

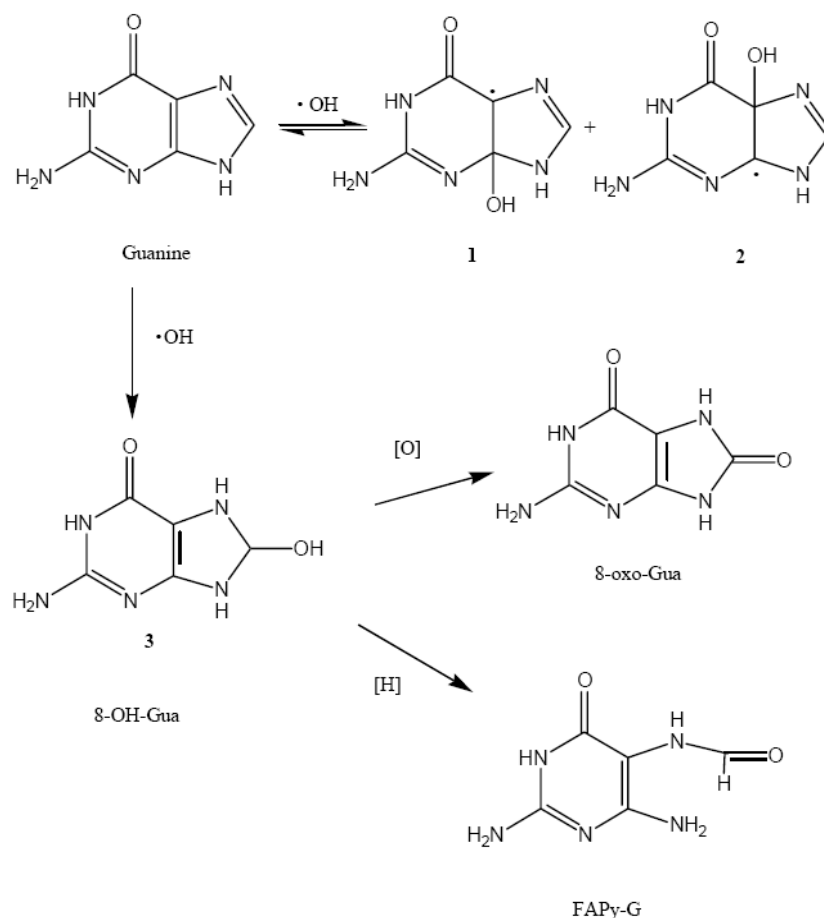


Figure 1.5 Schematic representation for the reaction of guanine with hydroxyl radicals

### 1.7.2 Carbon centered radicals

The study of DNA damage by carbon-centered radicals began with the discovery of enediyne antibiotics. There was EPR studies that the carbon radicals generated from dihydropyrazines are effective in causing DNA cleavage (Kashige *et al*, 2000). There are two ways carbon centered radicals can be formed *in vivo*. One is under conditions of high oxidative stress and the other is by abnormal metabolism of carbohydrates and amino acids brought about by genetic disorders.

It is thought that alkyl radicals are able to abstract hydrogen atoms from the sugar moiety in nucleotides leading to alkylation and consequently DNA damage. Carbon radicals induced DNA damage by attacking guanine and adenine bases of DNA forming 8-alkylpurines which can ultimately lead to DNA damage (Figure 1.6) (Maeda *et al*, 1974).

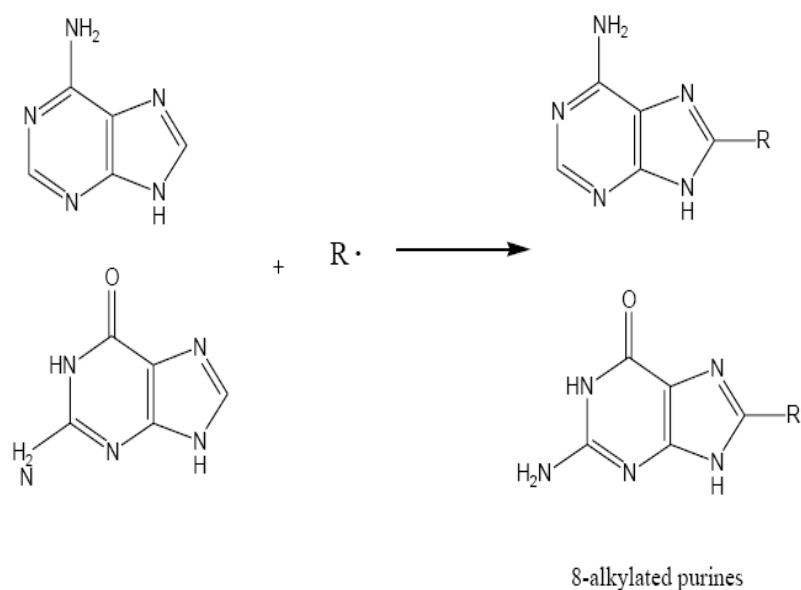


Figure 1.6 Schematic representation of carbon centered metabolites where R represents a carbon radical

### 1.8 Fenton-Menton reaction

Metals have special oxygen transfer properties which improve the use of hydrogen peroxide. Actually, metals have a strong catalytic power to generate highly reactive hydroxyl radicals ( $\cdot\text{OH}$ ). Below are the mechanism of Fenton-Menton reaction where M represents metal.

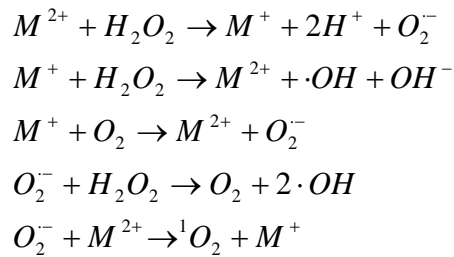


Figure 1.7 Mechanism of Fenton-Menton reaction (M represents metal)

### 1.9 MTT assay

MTT a standard colorimetric assay for measuring the activity of enzymes that reduce MTT to formazan, giving a purple color. This mostly happens in mitochondria, and as such it is in a measure of mitochondrial activity. It can also be used to determine cytotoxicity of potential medicinal agents and other toxic materials.

Yellow MTT 3-(4,5-Dimethylthiazol-2-yl)-2,5-diphenyltetrazolium bromide, a tetrazole) is reduced to purple formazan in the mitochondria of living cells. A solubilization solution (usually either dimethyl sulfoxide, an acidified ethanol solution, or a solution of the detergent sodium dodecyl sulfate in diluted hydrochloric acid) is added to dissolve the insoluble purple formazan product. The absorbance of this colored solution can be quantified by measuring absorbance at a certain wavelength (usually between 500 and 600 nm) by a spectrophotometer. The absorption maximum is dependent on the solvent employed.

This reduction takes place only when mitochondrial reductase enzymes are active, and therefore conversion is often used as a measure of viable (living) cells.

However, it is important to keep in mind that other viability tests sometimes give completely different results, as many different conditions can increase or decrease metabolic activity. Changes in metabolic activity can give large changes in MTT results although the number of viable cells maybe constant. When the amount of purple formazan produced by cells treated with an agent is compared with the amount of formazan produced by untreated control cells, the effectiveness of the agent in causing death, or changing metabolism of cells, can be deduced through the production of a dose-response curve.

#### 1.10 IC<sub>50</sub>

IC<sub>50</sub> is a measure of the effectiveness of a compound in inhibiting biological or biochemical function. Often, the compound in question is a drug candidate. This quantitative measure indicates how much of a particular drug or other substance (inhibitor) is needed to inhibit a given biological process (or component of a process, i.e. an enzyme, cell, cell receptor or microorganism) by half. In other words, it is the half maximal (50%) inhibitory concentration (IC) of a substance (50% IC, or IC<sub>50</sub>). It is commonly used as a measure of antagonist drug potency in pharmacological research. Sometimes, it is also converted to the pIC<sub>50</sub> scale (-log IC<sub>50</sub>), in which higher values indicate exponentially greater potency. According to the Food and Drug Administration, IC<sub>50</sub> represents the concentration of a drug that is required for 50% inhibition *in vitro*. It is comparable to an EC<sub>50</sub> for agonist drugs. EC<sub>50</sub> also represents the plasma concentration required for obtaining 50% of a maximum effect *in vivo* (Xu *et al.*,2004).



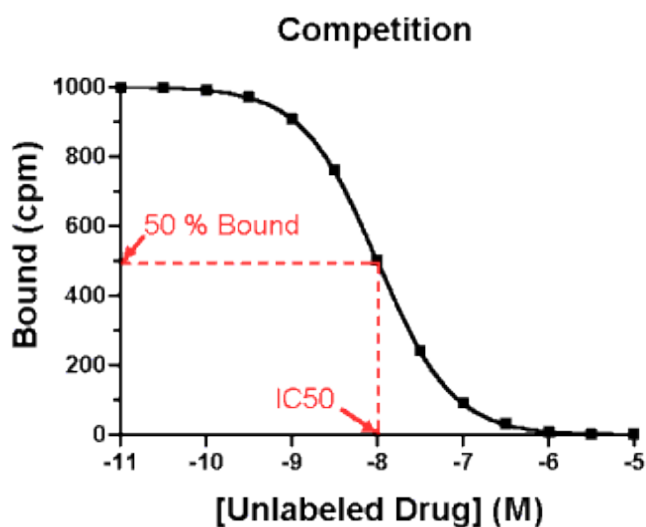


Figure 1.8 The graph of IC<sub>50</sub>

### 1.11 Objectives and scope of study

The objective of this research is to synthesize and characterize a series of complexes formed by the reaction of cobalt(II)chloride hexahydrate,  $\text{CoCl}_2 \cdot 6\text{H}_2\text{O}$  or zinc(II)acetate dihydrate,  $\text{Zn}(\text{CH}_3\text{COO})_2 \cdot 2\text{H}_2\text{O}$  with carboxylic acids.

1. To study the interaction of metal complexes with DNA
2. To study the DNA cleavage ability and the cytotoxic activity of metal complexes
3. To investigate the mechanism of the interaction between the metal complexes and DNA

## CHAPTER 2

### MATERIALS AND METHODS

#### 2.1 Reagents

Table 2.1 illustrates the melting points, purify, molecular weight and the suppliers for every chemical that used in the research. The chemicals were used without further purification.

Table 2.1 Chemicals used in the research

Name	Features			Supplier
	Melting Point (°C)	Purity (%)	Mr	
Cobalt(II) chloride hexahydrate	86°C	≥98.0%	237.93	Hamburg Chemical GmbH
Zinc(II) acetate dihydrate	100°C	≥97.5%	219.5	Fluka Chemika
2-Picolinic acid	135-136°C	98%	123.11	Fluka Chemika
Pyrazine-2-carboxylic acid	-21-22°C	99%	107.11	Aldrich
Malonic acid	132-135°C	≥98%	104.06	Fluka Chemika
Maleic acid	137-140°C	≥99%	116.08	Fluka Chemika
Glycine	<30°C	100%	75.07	Fisher Chemika
4-Aminobenzoic acid	187-189°C	99.5%	137.14	G.P.R.
Glycolic acid	75°C	97%	76.05	Fluka Chemika
Pyrazine-2,5-dicarboxylic acid dihydrate	190°C	≤97%	204.14	Fluka Chemika
Quinolinic acid	185°C	~99%	167.12	Fluka Chemika
3,5-Dinitrobenzoic acid	205°C	99.5%	212.12	BDH Chemicals

## 2.2 Experimental

Cobalt(II)chloride hexahydrate or zinc(II)acetate dihydrate was used as the starting material to prepare these complexes. Cobalt(II)chloride hexahydrate (1.00 g, 0.0042 mol) was dissolved in 20 mL of distilled water. The red solution was put into a two-neck round flask. Reagents in ratio of 1:2, starting material:ligand were used and refluxed for 3 hours.

Zinc(II)acetate dihydrate (1.00 g, 0.0046 mol) was dissolved in 20 mL of distilled water. The colourless solution was put into a two-neck round flask. Reagents in ratio of 1:2, starting material:ligand were used and refluxed for 3 hours.

All the ligands were dissolved in 30 mL of distilled water before mixed into the two-neck round flask.

## 2.3 Methods of characterization

### 2.3.1 Melting points

A Gallenkamp Variable Heater in a capillary tube in was used to determine the melting point of each complex. The complex was observed through a window of the heater and the temperature was recorded when the complex started to melt.

### 2.3.2 Conductivity measurement

The measurement was conducted on  $10^{-3}$  M of the complex solution by using the CyberScan 500 instrument.

### 2.3.3 Fourier transform infrared spectroscopy (FT-IR) analysis

The IR spectrum of the each complex was taken on a Perkin Elmer FTIR System 2000 spectrophotometer in the frequency range  $4000\text{--}400\text{ cm}^{-1}$  in the room temperature. Every dry analyte was ground with sodium bromide (KBr) in the ratio of 1:10 to obtain fine and evenly ground powder. The powder was used to form pellet using specific mould and pressed under 7 tonne by hydrolic press under vaccum.

### 2.3.4 Microanalysis CHN

A CHNS/O Analyzer (Perkin-Elmer Series II 2400) was used to determine the percentage of elements carbon, hydrogen and nitrogen.

### 2.3.5 Atomic absorption spectrometry (AAS) analysis

This analysis was carried out on a Perkin-Elmer Atomic Absorption Spectroscopy Model 310 to determine the quantitative value of cobalt and zinc in each complex. About 0.02 g of each complexes was dissolved in 10 mL of

concentrated nitric acid and diluted with 2% nitric acid until 50 mL in a volumetric flask.

#### 2.3.6 Ultraviolet-visible spectrometry (UV-Vis) analysis

About 0.02 g of each complexes was dissolved in distilled water. The UV-Visible spectra were measured on a Perkin-Elmer Lambda 35 in the range of 400-4000 nm. Dilution of each complexes was done until a nice peak obtained.

#### 2.3.7 Cyclic voltammetry (CV) analysis

This analysis was done by using BAS Epsilon. The measurements were made around  $10^{-3}$  M of the sample tested in distilled water using 0.1 M potassium chloride (KCl) as supporting electrolyte. A three-electrod (working, reference and counter) configuration cell was used in this analysis. A platinum electrode was used as counter electrode and all potentials were measured as the Ag/AgCl reference electrode. The sample solution was purged with nitrogen gas for 15 minutes to remove the oxygen from the solution and an atmosphere of nitrogen ( $N_2$ ) was maintained throughout eight cyclic voltammetric scans with the scan rate of 50 mV/s.

#### 2.3.8 Thermogravimetric (TGA) analysis

Thermogravimetric analysis of each complex was measured with a Mettler Toledo TGA/SDTA851e Thermal Gravimetric Analyzer. About 0.001-0.002 g of

each sample was placed in a platinum crucible and transferred to the heating furnace of the analyzer unit. The analysis was performed under a dynamic inert atmosphere ( $\text{N}_2$ ) with a flow rate of  $30 \text{ mL min}^{-1}$ . All samples were heated over the temperature range  $30\text{-}900 \text{ }^\circ\text{C}$  with heating rate of  $20 \text{ }^\circ\text{C min}^{-1}$ . All TGA data acquisitions and data processing were done using Mettler Toledo STARe version 8.10 software. The results were presented as differential thermal gravimetric curves.

### 2.3.9 X-ray crystallography

Complexes that were obtained as single crystals were determined on single crystal X-ray diffractometer equipped with monochromated  $\text{Mo-K}\alpha$  radiation ( $\lambda=0.71073 \text{ \AA}$ ) in order to reveal the crystal structure of the complexes. The intensity data for the titled complex was collected at  $100.0 \text{ K}$  using Bruker SMART APEX2 CCD or at  $273.0 \text{ K}$  using a Bruker SMART APEX CCD. The Oxford Cryosystem Cobra low-temperature attachment to SMART APEX2 CCD was also used to collect the low-temperature data. In addition, the data collected were refined using the program SAINT and a semi-empirical absorption correction was applied to the data using SADABS. The structure was solved by direct method and refined against  $F^2$  by full – matrix least squares using SHELXTL. Crystal data and experimental details of the structure determinations are listed in supplemental material.

### 2.3.10 DNA cleavage experiments

Agarose gel electrophoresis experiments were carried out on supercoiled plasmid pBR322 (4.4 kb). All samples in TAE buffer [40 mM Tris, 20 mM EDTA; pH 8.3; Tris=tris(hydroxymethyl)aminomethane; EDTA=disodium salt of ethylenediaminetetra-acetic acid] were incubated at 37 °C for 2 hours and then electrophoresed on 1 % agarose gel for 3 hours at 50 V. 0.0125 µg/µL DNA with the increasing concentration for each sample were incubated in the presence of a specified concentration of hydrogen peroxide (H<sub>2</sub>O<sub>2</sub>). At the end of electrophoresis, the gel was stained with ethidium bromide (EtBr) before being photographed under UV light using a Syngene Bio Imaging System.

In addition, the effect of hydroxyl radical scavengers (sodium azide, t-butanol, D-mannitol and DMSO) and hydrogen peroxide scavenger (KI) on the nucleolytic activity of these complexes were investigated. For each experiment, a 20 µL mixture consisting of the appropriate volumes of stock solution of DNA, complex dissolved in distilled water, additional buffer, scavengers and aqueous H<sub>2</sub>O<sub>2</sub> (last component added) was incubated at 37 °C for 2 hours before electrophoresis.

### 2.3.11 MTT assay

The human liver cancer cell line, HepG2 used in this study was obtained from American Type Culture Collection (ATCC, Manassas, VA, USA). The cells were grown in Dulbecco's modified Eagle's medium (DMEM; Invitrogen Co., Carlsbad, California, U.S.A) supplemented with 10 % heat-inactivated fetal calf serum (Invitrogen Co., Carlsbad, California, U.S.A), 100 µg/mL penicilin and 100 µg/mL

streptomycin (Flowlab, Sydney, Australia). Cells were kept in the logarithmic growth phase by routine passage every 2 or 3 days using 0.025 % trypsin-EDTA treatment.

MTT assay was used to test the cytotoxicity of sample complexes against human liver cells. MTT assay was performed in 96-flat bottom well plates. 100  $\mu$ L of cell ( $1 \times 10^5$  cell/mL) was seeded into each well except the outer surrounding wells (blank) of the plate and incubated for 24 hours. Then, 100  $\mu$ L of the dilution series of complex was added into each well and the plate was incubated for another 72 hours. The MTT solution was prepared at a concentration of 5 mg/mL in phosphate buffered saline (PBS). Later, 20  $\mu$ L of MTT was then added to each well and the plate was incubated for another 4 hours. The medium in the wells of the plate were removed and 200  $\mu$ L of DMSO was added to dissolve the formazan crystal (Xu *et al.*,2004). The absorbance of each well was measured in a microplate reader at 570 nm with a reference wavelength of 630 nm. The percentage of cell visibility was calculated with the formula:

$$\frac{\text{Average } A_{570} \text{ value for live cell (test)}}{\text{Average } A_{570} \text{ value for live cell (control)}} \times 100\%$$

The IC<sub>50</sub> value was obtained from the graphs of the complex was drawn.



## CHAPTER 3

### RESULTS AND DISCUSSION

#### 3.1 Characterization of diaquabis(2-pyrazinecarboxylato)cobalt(II) and diaquabis(2-pyrazinecarboxylato)zinc(II)

The complexes diaquabis(2-pyrazinecarboxylato)cobalt(II) and diaquabis(2-pyrazinecarboxylato)zinc(II) formed by the reaction of  $\text{CoCl}_2 \cdot 6\text{H}_2\text{O}$  and  $\text{Zn}(\text{CH}_3\text{COO})_2 \cdot 2\text{H}_2\text{O}$  with pyrazine-2-carboxylic acid are represented by Co(p-2c) and Zn(p-2c) respectively.

##### 3.1.1 Determination of physical properties

Orange crystals of Co(p-2c) and white crystals of Zn(p-2c) were obtained. Both these crystals are neutral by referring to the molar conductance table and soluble in polar solvents (Table 3.1.2). Co(p-2c) and Zn(p-2c) decomposed before reaching their melting points at 312.4-312.5 °C and 328.6-328.7 °C respectively (Table 3.1.1).

Table 3.1.1 The physical properties of Co(p-2c) and Zn(p-2c)

Complex	Co(p-2c)	Zn(p-2c)
Molecular Formula	$Co(C_5H_3O_2N_2)_2(H_2O)_2$	$Zn(C_5H_3O_2N_2)_2(H_2O)_2$
Molar Mass	341.15 g/mole	347.60 g/mole
Theoretical Value	1.43 g	1.60 g
Experimental Value	1.34 g	1.12 g
Yield	93%	70%
Appearance	Orange crystals	White crystals
Melting Points	312.4-312.5°C (Decompose)	328.6-328.7°C (Decompose)
Solubility	Dissolve in all polar solvents	Dissolve in all polar solvents
Conductivity	$79 \text{ cm}^2 \text{ ohm}^{-1} \text{ mol}^{-1}$	$17 \text{ cm}^2 \text{ ohm}^{-1} \text{ mol}^{-1}$

Table 3.1.2 Molar conductance,  $\Lambda$  of electrolyte solution at 25°C

Number of ion	Molar conductance, $\Lambda$
2	118-131
3	235-273
4	408-435
5	~560

### 3.1.2 Fourier transform infrared spectroscopy (FT-IR) analysis

For the correlation of the infrared spectra with the structure of metal carboxylates the difference between the asymmetric and symmetric carboxylate stretches [ $\Delta = \nu_{as}(\text{COO}^-) - \nu_s(\text{COO}^-)$ ] is often used. This value is approximately  $170 \text{ cm}^{-1}$  for ionic carboxylate group, indicated the group which does not interact strongly with metal ion (Deacon and Philip, 1980). In monodentate coordination the redistribution of electron density takes place, which shift the asymmetric carboxylate stretch,  $\nu_{as}(\text{COO}^-)$ , to higher wavenumbers in comparison to the ionic group. Consequently the  $\Delta$  value for monodentate carboxylate coordination is higher. While, bidentate coordination shifts the position of the asymmetric carboxylate stretch